Comparative quantum and semiclassical analysis of atom-field systems. I. Density of states and excited-state quantum phase transitions

M. A. Bastarrachea-Magnani,[1] S. Lerma-Hernández,[2,*] and J. G. Hirsch[1]

[1]*Instituto de Ciencias Nucleares, Universidad Nacional Autónoma de México, Apartado Postal 70-543, C.P. 04510 Mexico, Distrito Federal, Mexico*

[2]*Departamento de Física, Universidad Veracruzana, Circuito Aguirre Beltrán s/n, C.P. 91000 Xalapa, Veracruz, Mexico*

(Received 9 December 2013; published 3 March 2014)

We study the nonintegrable Dicke model and its integrable approximation, the Tavis-Cummings model, as functions of both the coupling constant and the excitation energy. Excited-state quantum phase transitions (ESQPT) are found analyzing the density of states in the semiclassical limit and comparing it with numerical results for the quantum case in large Hilbert spaces, taking advantage of efficient methods recently developed. Two different ESQPTs are identified in both models, which are signaled as singularities in the semiclassical density of states; one *static* ESQPT occurs for any coupling, whereas a *dynamic* ESQPT is observed only in the superradiant phase. The role of the unstable fixed points of the Hamiltonian semiclassical flux in the occurrence of the ESQPTs is discussed and determined. Numerical evidence is provided that shows that the semiclassical results describe very well the tendency of the quantum energy spectrum for any coupling in both models. Therefore, the semiclassical density of states can be used to study the statistical properties of the fluctuation in the spectra, a study that is presented in a companion paper.

DOI: 10.1103/PhysRevA.89.032101 PACS number(s): 03.65.Fd, 42.50.Ct, 64.70.Tg

I. INTRODUCTION

The Dicke Hamiltonian describes a system of $\mathcal{N}$ two-level atoms interacting with a single monochromatic electromagnetic radiation mode within a cavity [1]. In the language of quantum computation, it can also describe a set of $\mathcal{N}$ qubits from quantum dots, Bose-Einstein condensates, or QED circuits [2–5], interacting through a bosonic field. The Hamiltonian is very simple but not exactly solvable and continues to drive research into its properties. The most representative feature of the Dicke Hamiltonian is its second-order quantum phase transition (QPT) in the thermodynamic limit [6,7]. The ground state of the system goes from a normal to a superradiant state when the atom-field interaction reaches a critical value. This transition is an example of a quantum collective behavior [8]. The interest in solving the Dicke Hamiltonian for a finite $\mathcal{N}$ comes not only from the fact that it provides a good description for the systems manipulated in the laboratory, but from the close connection found between entanglement, QPTs, and quantum chaos [9–11]. Recently, Dicke-like Hamiltonians have attracted much attention because of the experimental realization of the superradiant phase transition in a BEC [12,13,14], while the debate around the validity of the description and its relation with the no-go theorem is far from closed [15–21]. In the thermodynamic limit (equivalent in the present models to the semiclassical limit), when the number of atoms $\mathcal{N}$ goes to infinity, the mean-field description becomes exact, and a Holstein-Primakoff expansion around it provides analytic solutions [9], which make it possible to extract the critical exponents for the ground-state energy per particle, the fraction of excited atoms, the number of photons per atom, their fluctuations, and the concurrence [9–11,22]. For a finite number of atoms $\mathcal{N}$, the model is, in general, nonintegrable, and care must be taken when the first order in the $1/\mathcal{N}$ expansion is employed because of its singular behavior around the phase transition [23–25].

The existence of an excited-state quantum phase transition (ESQPT) in the Dicke and Tavis-Cummings (TC) models was recently pointed out by Perez-Fernández *et al*. [26]. An ESQPT takes place along the energy spectrum, for fixed values of the Hamiltonian parameters. It is manifested by singularities in the level density, order parameters, and wave function properties [27]. The ESQPTs have been analyzed in several nuclear physics models [28] and could have important effects in decoherence [29] and the temporal evolution of quantum quenches [30]. Their relationship with the ground-state QPT is not completely clear, so the issue is open to current research.

We consider the nonintegrable Dicke model and its integrable approximation, the TC model, where the counter-rotating terms are neglected. These models are studied as functions of the coupling between atoms and field and as functions of the energy. The ESQPTs in these models are identified by studying the density of states in the semiclassical limit. We identify two ESQPT of different nature, a *static* one appearing for any coupling and a *dynamic* ESQPT which is present only in the superradiant phase. The role of the unstable fixed points, where abrupt changes in the available phase take place, in determining the ESQPTs is exposed. Analytic expressions for the density of states are obtained which coincide with those derived by Brandes recently [31]. We compare the semiclassical results with numerical results of the quantum model in large Hilbert spaces, taking advantage of efficient methods recently developed [22,32,33]. The comparison shows that the semiclassical results describe very well the tendency of the quantum spectra, in both the TC and the Dicke models and for the normal and superradiant phases. Consequently, the semiclassical density of states can be used to study the statistical properties of the quantum spectrum fluctuations, a study that is presented in the companion paper [34] of this series of two papers, where additionally the

*slerma@uv.mx

quantum results are compared with the onset of irregular trajectories in the semiclassical phase space.

The article is organized as follows. In Sec. II we present the Dicke and the TC Hamiltonians and summarize some of their properties. The classical Hamiltonians are described in Sec. III together with the analysis of the stable and unstable fixed points. In Sec. IV the available phase space volume as a function of coupling and energy is used to determine the semiclassical density of states. This density is compared with the quantum result in the same section. Section V contains the conclusions.

II. DICKE AND TAVIS-CUMMINGS HAMILTONIANS

The Dicke model describes the interaction between a system of $\mathcal{N}$ two-level atoms and a single mode of a radiation field within a cavity. The Hamiltonian is made of three parts: one associated to the monochromatic quantized radiation field, a second one to the atomic sector, and a last one which describes the interaction between them. The Dicke Hamiltonian can be written as

$$H_D = \omega a^\dagger a + \omega_0 J_z + \frac{\gamma}{\sqrt{\mathcal{N}}}(a + a^\dagger)(J_+ + J_-). \quad (1)$$

The frequency of the radiation mode is ω, which has an associated photon number operator $a^\dagger a$. For the atomic part ω_0 is the excitation energy; meanwhile, J_z, J_+, J_-, are collective atomic pseudospin operators which obey the SU(2) algebra. It holds that if $j(j+1)$ is the eigenvalue of $\mathbf{J}^2 = J_x^2 + J_y^2 + J_z^2$, then $j = \mathcal{N}/2$ (the pseudospin length) defines the symmetric atomic subspace which includes the ground state. γ is the interaction parameter. For atomic systems, it depends principally on the atomic dipolar moment. Besides, H_D commutes with the parity operator Π,

$$\Pi = e^{i\pi\Lambda}, \quad \text{with} \quad \Lambda = a^\dagger a + J_z + j. \quad (2)$$

The eigenvalues of the Λ operator, $\lambda = n + m + j$, are the total number of excitations, where n is the number of photons and $n_{\text{exc}} = m + j$ the number of excited atoms. As mentioned, in the thermodynamic limit a second-order QPT takes place when the interaction parameter reaches the critical value $\gamma_c = \sqrt{\omega\omega_0}/2$, separating the system into two regions: the normal phase ($\gamma < \gamma_c$) and the superradiant phase ($\gamma > \gamma_c$). In the normal phase the ground state has $\lambda = 0$, i.e., no photons and all atoms in their ground state. The superradiant phase is characterized by a macroscopic population of the upper atomic level and a comparable average photon number in the ground state of the system.

In general, for finite $\mathcal{N}$ the Dicke Hamiltonian is not integrable. However, it has two integrable limits: when $\gamma \to 0$ and when $\omega_o \to 0$ [32]. Moreover, when the coupling is weak it is possible to make the *rotating wave approximation* by ignoring the counter-rotating terms. The result is another integrable limit, the TC Hamiltonian [35]:

$$H_{\text{TC}} = \omega a^\dagger a + \omega_o J_z + \frac{\gamma}{\sqrt{\mathcal{N}}}(a J_+ + a^\dagger J_-). \quad (3)$$

The TC Hamiltonian is integrable because it commutes with the Λ operator. Its conserved eigenvalues λ define a set of subspaces where H_{TC} can be diagonalized independently. It also has a QPT in the thermodynamical limit, when the coupling has a critical value of $\gamma_{c,\text{TC}} = \sqrt{\omega_o\omega}$. For couplings $\gamma \leqslant \gamma_{c,\text{TC}}$, the ground state is the state with $\lambda = 0$, with no photons nor excited atoms, as in the Dicke model. When $\gamma > \gamma_{c,\text{TC}}$ the ground state has a certain $\lambda_c > 0$, which grows monotonically with γ. As an integrable approximation of the Dicke model, the TC model will help us to gain understanding of the connection between chaos, integrability, and the ESQPT.

We can write both models in one expression,

$$H = \omega a^\dagger a + \omega_0 J_z + \frac{\gamma}{\sqrt{\mathcal{N}}}[(a J_+ + a^\dagger J_-) + \delta(a^\dagger J_+ + a J_-)], \quad (4)$$

where $\delta = 0$ and 1 for the TC and Dicke models, respectively. With this parametrization the QPT's critical values are $\gamma_c = \sqrt{\omega_0\omega}/(1+\delta)$. From now on, we focus on the subspace with largest pseudospin, where $j = \mathcal{N}/2$.

III. CLASSICAL HAMILTONIANS

As discussed in previous works for the Dicke [23–25,31,36] and TC [37] models, many insights can be gained by studying the classical limit. Since we chose $\hbar = 1$, this limit is equal to the thermodynamical limit $j \to \infty$.

The classical versions of the Dicke and TC models can be obtained employing the *naive* substitution of the pseudospin variables by classical angular momentum ones ($J_i \to j_i$) and the substitution of the boson variables by a classical harmonic oscillator with $m\omega = 1$ ($\sqrt{2}a \to q + ip$ and $\sqrt{2}a^\dagger \to q - ip$). Recalling the relations $J_+ = J_x + iJ_y$ an $J_- = J_x - iJy$, we obtain

$$H_{cl} = \omega_o j_z + \frac{\omega}{2}(q^2 + p^2) + \frac{\gamma}{\sqrt{j}}[(1+\delta)q\, j_x - (1-\delta)p\, j_y]. \quad (5)$$

In Ref. [36] it was shown that the previous Hamiltonian is entirely equivalent to that obtained by using bosonic and SU(2) coherent states. The pseudospin variables satisfy the Poisson-bracket algebra $\{j_i, j_j\} = \epsilon_{ijk} j_k$. Canonical variables satisfying $\{P, Q\} = -1$ can be constructed from them as $P = j_z$ and $Q = \phi = \tan^{-1}(j_y/j_x)$, where ϕ is the azimuthal angle of the vector $\vec{j} = (j_x, j_y, j_z)$ whose magnitude is constant $|\vec{j}| = j$. In terms of the canonical variables, the classical Dicke and TC Hamiltonian reads

$$H_{cl} = \omega_o\, j_z + \frac{\omega}{2}(q^2 + p^2) + \gamma\sqrt{j}\sqrt{1 - \frac{j_z^2}{j^2}} \times [(1+\delta)\, q\cos\phi - (1-\delta)\, p\sin\phi]. \quad (6)$$

The associated classical equations of motion are

$$\frac{dq}{dt} = \frac{\partial H_{cl}}{\partial p} = \omega\, p - (1-\delta)\gamma\sqrt{j}\sqrt{1 - \frac{j_z^2}{j^2}}\sin\phi, \quad (7)$$

$$\frac{dp}{dt} = -\frac{\partial H_{cl}}{\partial q} = -\omega\, q - (1+\delta)\gamma\sqrt{j}\sqrt{1 - \frac{j_z^2}{j^2}}\cos\phi, \quad (8)$$

$$\frac{d\phi}{dt} = \frac{\partial H_{cl}}{\partial j_z} = \omega_o - \frac{\gamma j_z}{j^{3/2}\sqrt{1-\frac{j_z^2}{j^2}}} \times [(1+\delta)q\cos\phi - (1-\delta)p\sin\phi], \tag{9}$$

$$\frac{dj_z}{dt} = -\frac{\partial H_{cl}}{\partial \phi} = 2\gamma\sqrt{j}\sqrt{1-\frac{j_z^2}{j^2}} \times [(1+\delta)q\sin\phi + (1-\delta)p\cos\phi]. \tag{10}$$

The fixed points of the Hamiltonian flux correspond to the values (q_m, p_m, j_{zm}) which produce the simultaneous cancellation of the four derivatives. Two of them are present for any value of the coupling constant γ,

$$(q_m, p_m, j_{zm}) = (0,0,\pm j).$$

Note that $j_z = \pm j$ correspond to the north and south poles of the pseudospin sphere where the value of the azimuthal angle is irrelevant. If we evaluate the Hamiltonian in the previous fixed points, we obtain, respectively and for any coupling, the energies $\epsilon = \pm 1$, where we have, conveniently, rescaled the energy as

$$\epsilon \equiv \frac{E}{\omega_o j}. \tag{11}$$

The nature of the previous fixed points is as follows, the point $(q_m, p_m, j_{zm}) = (0,0,+j)$ is an unstable fixed point for any value of the coupling γ, whereas the point $(q_m, p_m, j_{zm}) = (0,0,-j)$ is a stable fixed point for couplings $\gamma \leqslant \gamma_c$ that becomes unstable for couplings $\gamma > \gamma_c$. It represents the semiclassical description of the ground state in the normal phase, with no photons and no excited states.

For couplings larger than the critical one, new stable points emerge whose properties depend on the model we are considering, Dicke ($\delta = 1$) or TC ($\delta = 0$). For the Dicke model two degenerate stable fixed points emerge which are given by

$$\begin{aligned}(q_m, p_m)_\pm &= \left[\mp\frac{2\gamma\sqrt{j}}{\omega}\sqrt{1-\left(\frac{\gamma_c}{\gamma}\right)^4}, 0\right], \\ (\cos\phi_m, j_{zm})_\pm &= \left[\pm 1, -j\left(\frac{\gamma_c}{\gamma}\right)^2\right],\end{aligned} \tag{12}$$

whereas for the integrable TC model a continuous set of stable fixed points parametrized by the angle $\phi \in [0, 2\pi)$ appear, which are given by

$$\begin{aligned}(q_m, p_m) &= \frac{\gamma\sqrt{j}}{\omega}\sqrt{1-\left(\frac{\gamma_c}{\gamma}\right)^4}(-\cos\phi, \sin\phi), \\ j_{zm} &= -j\left(\frac{\gamma_c}{\gamma}\right)^2.\end{aligned} \tag{13}$$

The continuous set of fixed points in the TC model is a consequence of the symmetry associated with the conserved quantity Λ (2), whose classical version is $\Lambda_c = (q^2 + p^2)/2 + j_z + j$.

To better visualize the properties of the fixed points in both models, we construct energy surfaces in terms of the pseudospin variables j_z and ϕ. Equating to zero Eqs. (7) and (8) we obtain $\sqrt{j}\omega p = (1-\delta)\gamma\sqrt{j^2 - j_z^2}\sin\phi$ and $\sqrt{j}\omega q = -(1+\delta)\gamma\sqrt{j^2 - j_z^2}\cos\phi$; by substituting these results in the Hamiltonian we obtain a semiclassical expression for the energy as a function of j_z and ϕ,

$$\frac{E(j_z,\phi)}{\omega_o j} = \frac{j_z}{j} - \frac{\gamma^2}{2\gamma_c^2}\left(1-\frac{j_z^2}{j^2}\right)\left[1 - \frac{4\delta}{(1+\delta)^2}\sin^2\phi\right]. \tag{14}$$

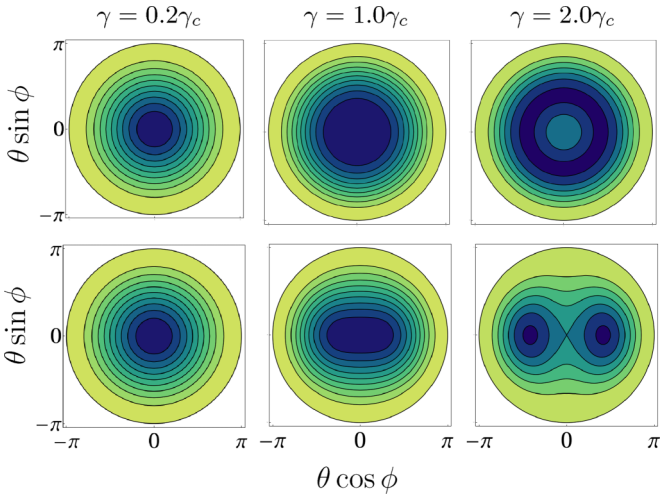

FIG. 1. (Color online) Contour plots of the energy surface [Eq. (14)] for the TC (top) and Dicke (bottom) models for three different couplings. Dark tones indicate low values of the energy. Angular variables of the pseudospin $\vec{j}$ are used: ϕ is the azimuthal angle and θ is the zenith angle measured with respect to the south pole ($j_z = -j\cos\theta$).

For the TC model ($\delta = 0$) the energy surface is independent on the angle ϕ. In Fig. 1 contour plots of the energy surface are shown for the TC and Dicke models and for three different values of the couplings. Variables ϕ and θ are used, where θ is the zenith angle of $\vec{j}$ measured with respect to the south pole ($j_z = -j\cos\theta$). Because of the symmetry Λ of the TC model, its contours are circular for any coupling. For small couplings the energy surfaces of the Dicke and TC models are almost indistinguishable, with circular contours and a global minimum in the south pole ($\theta = 0$). For couplings close but below the critical value, the global minimum is yet the south pole but the contours begin to exhibit deformation in the Dicke model. For couplings above γ_c, the south pole becomes a local maximum for the TC model and a saddle point in the Dicke model. Besides, according to Eq. (13), two degenerate minima appear in the case of the Dicke model in $\phi = 0$ and π, whereas for the TC model, the energy surface takes a Mexican hat form with a continuous set of minima circularly located around the south pole, which is related to a Goldstone mode [38,39].

The energy minimum is obtained by evaluating the Hamiltonian in the stable fixed points. The result, valid for both the TC and Dicke models, is given by

$$\epsilon_{\min} \equiv \frac{E_{\min}}{\omega_o j} = \begin{cases} -1 & \text{for} \quad \gamma \leqslant \gamma_c, \\ -\frac{1}{2}\left(\frac{\gamma_c^2}{\gamma^2} + \frac{\gamma^2}{\gamma_c^2}\right) & \text{for} \quad \gamma > \gamma_c.a \end{cases} \tag{15}$$

This function is shown in Fig. 2, together with cuts of the energy surface (14) for $\sin\phi = 0$. The cuts are shown as

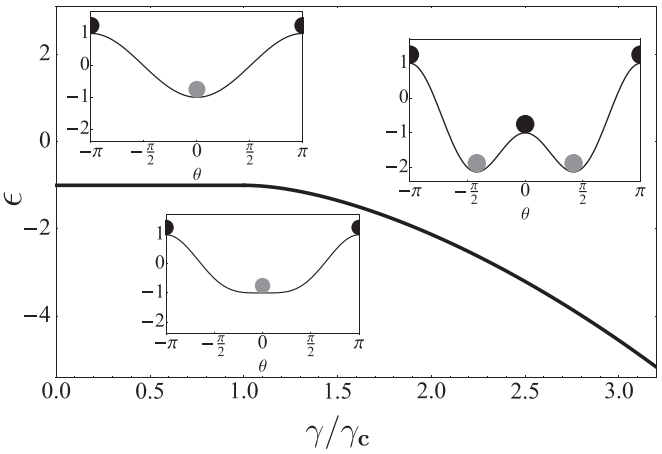

FIG. 2. Scaled energy minimum [$\epsilon_{\min} \equiv E_{\min}/(\omega_o j)$] as a function of the coupling constant measured with respect to the critical value (γ/γ_c). In the insets three typical energy surfaces are shown for couplings, from left to right, $\gamma/\gamma_c = 0.2$, 1.0, and 2.0. Stable and unstable fixed points are signaled by gray and black circles, respectively. The angle θ is that formed by the pseudospin $\vec{j}$ and the negative z axis.

a function of the angle θ, where positive and negative θ correspond, respectively, to $\phi = 0$ and $\phi = \pi$. The fixed points and their respective nature can be easily visualized in these energy surfaces, and it is apparent that the transition that takes place in the critical coupling is a second-order pitchfork transition.

IV. DENSITY OF STATES

The stable fixed points of the classical TC and Dicke models (gray dots in Fig. 2), identified and discussed in the previous section, are useful to understand the behavior of the energy minimum, associated with the ground-state QPT in the quantum version of the models. Likewise, the unstable ones (black dots in Fig. 2) are benchmarks in the energy space which indicate abrupt changes in the behavior of the available phase space. These changes, whose quantum analogs are referred to as ESQPT [27], deserve a detailed analysis which is conducted in the following.

A. Classical volume of the available phase space

The volume of the available phase space for a given energy (E), which divided by $(2\pi\hbar)^2$ with $\hbar = 1$, is given by

$$\nu(E) = \frac{1}{(2\pi)^2} \int dq\, dp\, d\phi\, dj_z\, \delta(E - H_{cl}(q,p,\phi,j_z)). \quad (16)$$

The previous expression, according to the Gutzwiller's trace formula [40], is the semiclassical approximation of the quantum density of states. Recently, this volume was evaluated as an inverse Laplace transform of the partition function of the model [31]. Alternatively, we calculate the integral directly. The quadratic nature of the Hamiltonians for the boson variables makes it possible to perform the integrals over p and q, giving (see Appendix A)

$$\nu(E) = \frac{1}{2\pi\omega} \int dj_z \int d\phi. \quad (17)$$

To evaluate this expression we need to know the range of the pseudospin variables for a given energy E. Here we present the main results; the details are shown in Appendix A. For the TC model the Λ symmetry allows the angle variable ϕ take any value in the interval $[0,2\pi)$ for any coupling and energy. Therefore, Eq. (17) reduces to $\nu(E) = (1/\omega)\int dj_z$. On the other hand, the values the variable j_z can take depend on coupling and energy. Three different energy regimes are identified (a) $1 < \epsilon$, (b) $-1 \leqslant \epsilon \leqslant 1$, and (c) $\epsilon_o \leqslant \epsilon < -1$, with $\epsilon_o = -\frac{1}{2}(\frac{\gamma_c^2}{\gamma^2} + \frac{\gamma^2}{\gamma_c^2})$. The latter interval appears only in the superradiant phase ($\gamma \geqslant \gamma_c$). For energies $1 < \epsilon$ the whole pseudospin sphere is available: $j_z \in [-j, j]$ and, consequently, the available phase space volume saturates ($\nu = 2j/\omega$). For energies $-1 \leqslant \epsilon \leqslant 1$, the j_z variable takes values only in the interval $[-j, jy_+]$ with $y_{\pm}$, ($|y_+| < 1$) given by

$$y_{\pm} = \left[-\frac{\gamma_c^2}{\gamma^2} \pm \frac{\gamma_c}{\gamma}\sqrt{2(\epsilon - \epsilon_o)}\right]. \quad (18)$$

For couplings above the critical value, $\gamma > \gamma_c$, according to Eq. (15), the range of possible energies extends until $\epsilon_o < -1$. For the interval $\epsilon \in [\epsilon_o, -1)$ the south pole of the pseudospin sphere ($j_z = -j$) is inaccessible and the j_z variable is restricted to the interval $jy_- \leqslant j \leqslant jy_+$, with $|y_{\pm}| < 1$ given by Eq. (18). With the previous results the classical approximation for the density of states in the TC model can be easily obtained:

$$\frac{\omega}{2j}\nu(\epsilon) = \begin{cases} \frac{\gamma_c}{\gamma}\sqrt{2(\epsilon - \epsilon_0)}, & \epsilon_0 \leqslant \epsilon < -1, \\ \frac{1}{2}\left[1 - \frac{\gamma_c^2}{\gamma^2} + \frac{\gamma_c}{\gamma}\sqrt{2(\epsilon - \epsilon_0)}\right], & |\epsilon| \leqslant 1, \\ 1, & \epsilon > 1. \end{cases} \quad (19)$$

The volume of the available phase space for the TC model for three different couplings, as a function of the energy, is shown in the top panels of Fig. 3. The available phase space in the pseudospin space for different energy regimes is also shown above the curves, indicated by gray zones in the polar plots, $1 + (j_z/j)$ vs ϕ. The changes in the available phase space that occur at energies $\epsilon = \mp 1$ are clearly indicated by discontinuities in the derivatives $\nu'(\epsilon)$, shown as insets at the bottom of each panel.

For the Dicke model, the range of the j_z variable is (see Appendix A) given by the same expressions as in the TC model: $j_z \in [jy_-, jy_+]$ for $\epsilon_o \leqslant \epsilon < -1$, $j_z \in [-j, jy_+]$ for $-1 \leqslant \epsilon \leqslant 1$, and $j_z \in [-j, j]$ for $1 < \epsilon$. On the other hand, since the Λ symmetry is broken for the Dicke model, the available range of the ϕ variables depends on coupling and energy. For energies $1 < \epsilon$, as in the TC model, the available pseudospin phase space saturates and ϕ takes values in the whole interval $[0,2\pi)$. For energies $-1 \leqslant \epsilon \leqslant 1$ the whole interval $[0,2\pi)$ is accessible only if $-j \leqslant j_z \leqslant \epsilon j$. For $j\epsilon < j_z \leqslant jy_+$ the ϕ variable is restricted by the condition

$$2j\frac{\gamma_c^2}{\gamma^2}\frac{(j_z - j\epsilon)}{(j^2 - j_z^2)} \leqslant \cos^2\phi \leqslant 1. \quad (20)$$

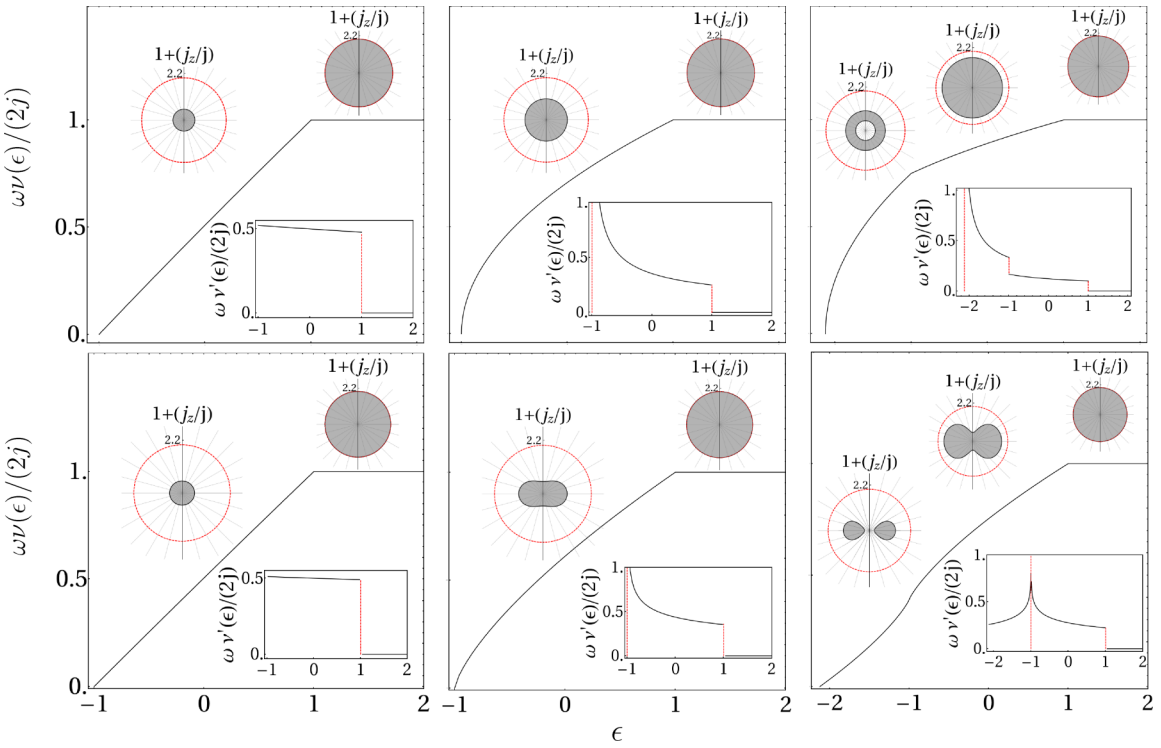

FIG. 3. (Color online) Scaled available phase space volume $\omega\nu(\epsilon)/(2j)$ for the TC model (top) and Dicke model (bottom) as a function of $\epsilon \equiv E/(\omega_o j)$, for couplings $\gamma = 0.2\gamma_c$ (left), $\gamma = \gamma_c$ (middle), and $\gamma = 2\gamma_c$ (right). The derivatives of $\nu(\epsilon)$ are shown as insets at the bottom right of each panel. Polar plots, $1 + (j_z/j)$ vs ϕ, of the available pseudospin phase space (gray zones) for representative energies ($\epsilon = -0.5$ and 1.5) are shown in the upper part of the panels. In the rightmost panels a third polar plot is added depicting the available phase space in the superradiant region, for $\epsilon = -2.0$ (TC, top) and $\epsilon = -1.6$ (Dicke, bottom).

Finally, for $\epsilon_o \leqslant \epsilon < -1$ (possible only in the superradiant phase $\gamma > \gamma_c$), the ϕ variable is restricted by the same condition (20). Having identified the range of the pseudospin variable, it is straightforward to obtain an expression for $\nu(\epsilon)$ for the Dicke model,

$$\frac{\omega}{2j}\nu(\epsilon) = \begin{cases} \frac{1}{\pi}\int_{y_-}^{y_+} \arccos\sqrt{\frac{2\gamma_c^2(y-\epsilon)}{\gamma^2(1-y^2)}}\,dy, & \epsilon_0 \leqslant \epsilon < -1, \\ \frac{\epsilon+1}{2} + \frac{1}{\pi}\int_{\epsilon}^{y_+} \arccos\sqrt{\frac{2\gamma_c^2(y-\epsilon)}{\gamma^2(1-y^2)}}\,dy, & |\epsilon| \leqslant 1, \\ 1, & \epsilon > 1, \end{cases} \tag{21}$$

where $y_\pm$ is given by (18).

The previous expression for the available phase space volume is plotted in Fig. 3 for three couplings as a function of the energy, in the bottom panels. The available pseudospin phase space for energies in the different regimes is also shown above the curves as gray areas in the polar plots. The changes in the available phase space occurring at energies $\epsilon = \mp 1$ are evident as discontinuities and divergences in the derivative $\nu'(\epsilon)$. Observe that for small couplings ($\gamma = 0.2\gamma_c$, left) the Dicke and TC curves are very similar, but they differ clearly at the critical coupling, where the available regions in the Dicke model are highly deformed. The differences are more dramatic in the superradiant phase $\gamma > \gamma_c$: While a discontinuity in the first derivative occurs at $\epsilon = -1$ for the TC model, the nonanalytic behavior of the derivative of $\nu(\epsilon)$ in the Dicke model is a logarithmic divergence [31]. This behavior can be understood by looking at the geometry of the available phase space in both models. In the TC model the available phase consists of a single circularly symmetric connected region, but in the Dicke model it consists of two disconnected regions for $\epsilon < -1$, which touch each other in the saddle point at $\epsilon = -1$ and merge for larger energies $\epsilon > -1$. In the next two sections, the previous classical approximations for the density of states are compared with the results coming from diagonalizing the Hamiltonian of the TC and Dicke quantum models.

B. Quantum density of states in the Tavis-Cummings model

The basis in which the TC Hamiltonian is diagonalized, for fixed j, can be labeled by λ and m. For a given value of λ, the number of states in each subspace is $N_{st}(\lambda) = \min(\lambda + 1, 2j + 1)$. This number of states grows linearly with λ up to $\lambda_0 = 2j$, and from that value on it remains fixed in $2j + 1$. It represents a *static* change in the density of states which is always present. The eigenstates of $H_{\rm TC}$ can be classified as $E(i,\lambda)$, $i = 1$, $N_{st}(\lambda)$. To obtain a complete energy spectrum up to an energy $E_{\rm ref}$, all subspaces up to $\lambda_{\rm max}$ must be included, where $\min(E(i,\lambda_{\rm max})) > E_{\rm ref}$.

We have studied the resonant case, $\omega = \omega_o = 1$, which has $\gamma_{c,\rm TC} = 1.0$. Selecting $\mathcal{N} = 200$ ($j = 100$), $\lambda_{\rm max} = 2000$ is enough to provide the complete energy spectrum up to the scaled energy $\epsilon = 6.4$ for $\gamma = \gamma_{c,\rm TC}$, with 264 000 states, and up to $\epsilon = 3.3$ for $\gamma = 2\gamma_{c,\rm TC}$ with 160 000 states.

Using n as the order number in which each state with energy E appears in the energy spectrum, in top row of Fig. 4 we present $\frac{n}{\mathcal{N}}$ as function of ϵ for (a) $\gamma = \gamma_{c,\rm TC}$,

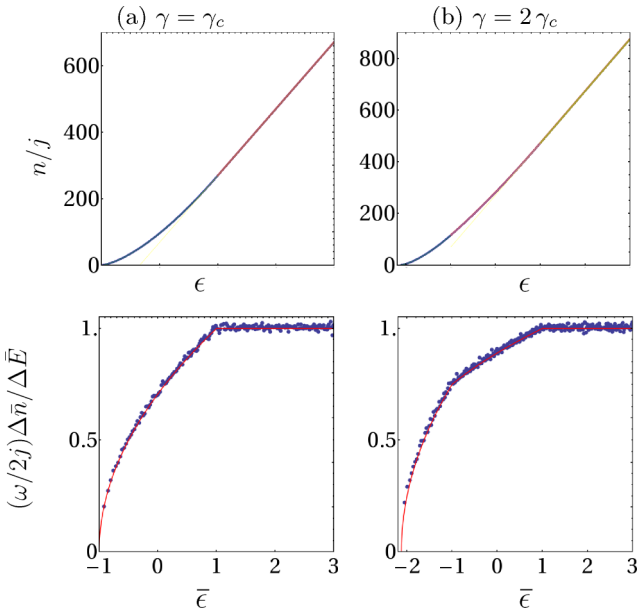

FIG. 4. (Color online) (Top row) $\frac{n}{j}$ as a function of ϵ for (a) $\gamma = \gamma_c$ and (b) $\gamma = 2\gamma_c$. (Bottom row) Averaged quantum density of states, $\frac{\omega}{2j}\frac{\Delta\bar{n}}{\Delta\bar{E}}$ (blue points), in the TC model as a function of $\bar{\epsilon}$ for (a) $\gamma = \gamma_c$ and (b) $\gamma = 2\gamma_c$. The continuous red lines depict the semiclassical results.

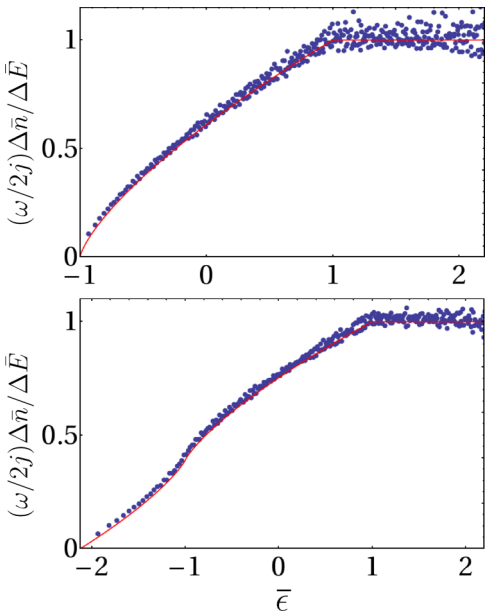

FIG. 5. (Color online) Averaged quantum density of states, $\frac{\omega}{2j}\frac{\Delta\bar{n}}{\Delta\bar{E}}$ (blue points), in the Dicke model as a function of $\bar{\epsilon}$ for $\gamma = \gamma_c$ (top) and $\gamma = 2\gamma_c$ (bottom). The continuous red lines indicate the corresponding semiclassical results.

(b) $\gamma = 2\gamma_{c,\mathrm{TC}}$. Notice the three regions, displayed with different colors, corresponding to $\epsilon_0 \leqslant \epsilon < -1$, $|\epsilon| \leqslant 1$, and $\epsilon > 1$ in Fig. 4(b), while in Fig. 4(a) there are only two, because the ground-state energy is $\epsilon_{\mathrm{GS}} = E_{\mathrm{GS}}/(\omega_o j) = -1$. The thin lines inside are the fits in each region, inspired in their functional form in the integrals of $\nu(\epsilon)$. It is worth mentioning that the derivatives of the fitted function coincide with $\nu(\epsilon)$, with differences of the order $\frac{1}{\mathcal{N}}$.

While the curves presented in the top row of Fig. 4 seem to be smooth, obtaining their first derivative as finite differences in order to estimate the quantum density of states is tricky because the fluctuations obscure the results. To overcome this difficulty we have taken averages of the energy $\bar{E}(\bar{n})$ over intervals of 600 levels, with average number of state $\bar{n}$. From these averaged quantities we obtain the average derivative $\frac{\Delta\bar{n}}{\Delta\bar{E}}$, displayed in the bottom row of Fig. 4.

The continuous red curves representing $\nu(\epsilon)$ overlap nicely with the averaged numerical results, presented as points. The *static* excited-state phase transition at $\epsilon = 1$ is present in both cases, while the *dynamic* phase transition at $\epsilon = -1$ can be observed, very clearly, for the superradiant case $\gamma = 2\gamma_{c,\mathrm{TC}}$.

C. Quantum density of states in the Dicke model

We repeat some of the calculations we did in the case of the TC model for the Dicke model, but in this case we must be careful with the convergence of the numerical solutions because the model is not integrable. We diagonalize numerically the Dicke Hamiltonian employing an extended bosonic coherent basis (see Appendix B), which let us obtain a significative part of the energy spectra with a small truncation or cutoff [22,32,33]. For a given truncation we can estimate for each individual excited state a lower bound of the numerical precision in the wave function, as pointed out in Appendix B. In this way we can monitor that each eigenstate has converged up to some chosen significative figures. We have selected the resonant case $\omega = \omega_o$, with $\mathcal{N} = 80$ ($j = 40$).

For the Dicke model the fluctuations in energy are smaller than in the TC, and the averages of the energy $\bar{E}(\bar{n})$ are taken over intervals of 20 levels, with average number of state $\bar{n}$. From these averaged quantities we obtain the average derivative $\frac{\Delta\bar{n}}{\Delta\bar{E}}$, displayed in Fig. 5.

The continuous red curves plot $\nu(\epsilon)$, the same ones plotted in Fig. 3, which also in this case overlap nicely with the averaged numerical results, presented as points. The *static* ESQPT at $\epsilon = 1$ is present in both cases, while the *dynamic* phase transition at $\epsilon = -1$ can be observed, very clearly, for the superradiant case $\gamma = 2\gamma_c$.

The numerical evidence provided in this section shows that the semiclassical density of states describes correctly the tendency of the quantum spectra of the TC and Dicke models, in both the normal and the superradiant phases. Consequently, the semiclassical result can be safely used to perform the so-called unfolding of the quantum spectra and study the statistical properties of quantum fluctuations. It is well known that the properties of these fluctuations are the same as those of different random matrix ensembles depending on the dynamic of the underlying semiclassical model: the Gaussian diagonal ensemble (GDE) for quasi-integrable or regular dynamics, and the Gaussian orthogonal ensemble (GOE) for chaotic dynamics with time-invariant symmetry. This analysis is performed in the companion paper [34] to this one.

V. CONCLUSIONS

Using both a semiclassical analysis and results of an efficient numerical procedure to diagonalize the quantum

Hamiltonians, we have studied the Dicke and TC models in the space of couplings and excitation energies. We have focused on a global property in the energy-coupling space: the ESQPTs or singular behavior of the density of states.

Analytical results for the semiclassical approximation to the density of sates were derived by calculating the volume of the available phase space for a given coupling and energy. From the classical analysis, two different unstable fixed points of the Hamiltonian flux can be identified. The first one located at the north pole of the pseudospin sphere appears for any coupling. The second one appears only in the superradiant phase and is located at the south pole of the pseudospin sphere. The role of these unstable fixed points in relation to the occurrence of the ESQPTs was discussed and established. The unstable points are benchmarks in the energy space which indicate an abrupt change in the available phase space. The two unstable fixed points produce two kinds of ESQPTs. The first one, referred to as *static* ESQPT, occurs for any coupling at energy $E/(\omega_o j) = 1$. At this energy the whole pseudospin sphere becomes available for the system. The second ESQPT, referred to as *dynamic*, occurs only for couplings larger than the critical one at energies $E/(\omega_o j) = -1$. This transition occurs when the top of the double well (Dicke) or Mexican hat (TC) potential that develops in the superradiant phase is attained. The abrupt changes in the available phase space are reflected in the classical density of states as nonanalytic behavior of its first derivative. For the integrable TC model, the first derivative shows a discontinuity for both the *static* and the *dynamic* ESQPTs. For the Dicke model the *static* ESQPT is equally reflected by a discontinuity of the first derivative, but the *dynamic* ESQPT is associated with a logarithmic divergence of the first derivative. For the quantum case, finite systems [$\mathcal{N} = 200$ (TC) and $\mathcal{N} = 80$ (Dicke)] were diagonalized in large energy regions which include all the regimes identified in the semiclassical approximation. The tendency of the quantum spectra was obtained by averaging the energy and the number of state index, over intervals of 600 (TC) and 20 (Dicke) contiguous states. After this average procedure, it was shown that the quantum results overlap perfectly with the semiclassical density of states. This result confirms that the semiclassical approximation is appropriate for performing the unfolding of the quantum spectrum and, consequently, for studying the properties of its fluctuations [34].

ACKNOWLEDGMENTS

We thank P. Stránsky and P. Cejnar for many useful and interesting conversations. This work was partially supported by CONACyT- México, DGAPA-UNAM, and DGDAEIA-UV through the "2013 Internal Call for Strengthening Academic Groups" (Academic Group No. UV-CA-320).

APPENDIX A: AVAILABLE PHASE SPACE FOR A GIVEN E

Here, we perform the boson variables (q and p) integration of [with $H_{cl}(q,p,\phi,j_z)$ defined in Eq. (6)]

$$\nu(E) = \frac{1}{(2\pi)^2}\int dj_z\, d\phi\, dp\, dq\, \delta(E - H_{cl}(q,p,\phi,j_z))$$

and determine the range of the pseudospin variables for a given energy and coupling. The q integration is straightforward by using the properties of the Dirac δ,

$$\nu(E) = \frac{1}{(2\pi)^2}\int dj_z\, d\phi\, dp\, dq \left[\frac{\delta(q-q_+)}{|\partial H_{cl}/\partial q|_{q_+}} + \frac{\delta(q-q_-)}{|\partial H_{cl}/\partial q|_{q_-}}\right],$$

where $q_\pm$ are the roots of the quadratic equation $E - H_{cl}(q,p,\phi,j_z) = 0$,

$$\omega q_\pm = -\gamma\sqrt{j}\cos\phi\sqrt{1-\frac{j_z^2}{j^2}}(1+\delta) \pm \sqrt{-\omega^2 p^2 + b\,p + c}, \tag{A1}$$

with the coefficients b and c given by

$$b = 2\omega\gamma\sqrt{j}\sin\phi\sqrt{1-\frac{j_z^2}{j^2}}(1-\delta)$$

and

$$c = \gamma^2 j\cos^2\phi\left(1-\frac{j_z^2}{j^2}\right)(1+\delta)^2 + 2\omega(E-\omega_o j_z).$$

Evaluating the derivatives, one obtains $|\partial H_{cl}/\partial q|_{q_+} = |\partial H_{cl}/\partial q|_{q_-} = \sqrt{-\omega^2 p^2 + bp + c}$; then the q integration yields

$$\nu(E) = \frac{1}{(2\pi)^2}\int dj_z\, d\phi\, dp\, \frac{2}{\sqrt{-\omega^2 p^2 + bp + c}},$$

with the limits in the variables j_z, ϕ, and p determined by the condition $-\omega^2 p^2 + bp + c \geqslant 0$. The p integration is easily performed by writing

$$-\omega^2 p^2 + bp + c = \omega^2(p_+ - p)(p - p_-),$$

with $p_\pm$ the roots ($p_- \leqslant p_+$) of the quadratic polynomial $-\omega^2 p^2 + bp + c = 0$,

$$\begin{aligned}\nu(E) &= \frac{2}{\omega(2\pi)^2}\int dj_z \int d\phi \int_{p_-}^{p_+} dp \frac{1}{\sqrt{(p_+ - p)(p - p_-)}} \\ &= \frac{2\pi}{\omega(2\pi)^2}\int dj_z \int d\phi.\end{aligned}$$

The previous result is valid provided that the roots $p_\pm$ are real, which, in turn, occurs only if the maximum of the polynomial $-\omega^2 p^2 + bp + c$ is greater than or equal to zero:

$$\frac{b^2}{4\omega^2} + c \geqslant 0.$$

By substituting the values of b and c, the previous condition reads

$$\frac{\gamma^2}{2\gamma_c^2}(1-y^2)\left[\frac{(1-\delta)^2}{(1+\delta)^2}\sin^2\phi + \cos^2\phi\right] \geqslant y - \epsilon, \tag{A2}$$

with $\gamma_c = \sqrt{\omega\omega_o}/(1+\delta)$, and we have used the variables $y \equiv j_z/j$ ($|y| \leqslant 1$) and $\epsilon \equiv E/(\omega_o j)$. The previous condition determines the range of the pseudospin variables for a given energy ϵ. For the TC model ($\delta = 0$) the previous condition is independent of ϕ and simplifies to

$$\frac{\gamma^2}{2\gamma_c^2}(1-y^2) \geqslant y - \epsilon;$$

therefore, no restriction for the variable ϕ occurs and it can take any value in the interval $[0,2\pi)$. If $\epsilon > 1$ the previous condition is satisfied in the whole interval $y \in [-1,1]$, in this case the whole pseudospin sphere is accessible. For $-1 \leqslant \epsilon \leqslant 1$, the condition is satisfied only for $y \in [-1,y_+]$ ($y_+ < 1$), where $y_\pm$ are the roots of $\frac{\gamma^2}{2\gamma_c^2}(1-y^2) = y - \epsilon$, given in Eq. (18). Finally, for energies $\epsilon < -1$, the condition is satisfied in the interval $y \in [y_-,y_+]$ ($|y_\pm| < 1$) only if $\gamma > \gamma_c$ and $\epsilon \geqslant \epsilon_o$, where $\epsilon_o < -1$ is the classical ground-state energy in the superradiant phase defined immediately after Eq. (18).

For the Dicke model ($\delta = 1$) the condition (A2) is

$$\frac{\gamma_c^2}{\gamma^2}\frac{2(y-\epsilon)}{1-y^2} \leqslant \cos^2\phi; \tag{A3}$$

clearly, this condition constrains the values the ϕ variable can take. If $\epsilon > 1$ the condition is satisfied for the whole pseudospin sphere $y \in [-1,1]$ ($j_z \in [-j,j]$) and $\phi \in [0,2\pi)$. For energies satisfying $-1 \leqslant \epsilon \leqslant 1$, similar to the TC case, the condition can be satisfied only for $y \in [-1,y_+]$, but here, contrary to the TC case, a restriction to the ϕ variable appears as follows: If $y \in [-1,\epsilon]$, ϕ takes values in the whole interval $[0,2\pi)$, but if $\epsilon < y \leqslant y_+$ the angular variable is restricted by the condition (A3), which is satisfied for values in intervals around $\phi = 0$ and $\phi = \pi$.

Finally, as in the TC case, for energies $\epsilon < -1$, the condition can be satisfied in the interval $y \in [y_-,y_+]$ only if $\gamma > \gamma_c$ and $\epsilon \geqslant \epsilon_o$, where $\epsilon_o < -1$ is the classical ground-state energy in the superradiant phase. However, now, contrary to the TC case, the angular variable is restricted by the condition (A3).

APPENDIX B: NUMERICAL SOLUTIONS AND PRECISION IN THE WAVE FUNCTION

We use an extended bosonic coherent basis in order to diagonalize the Dicke Hamiltonian [22,32,33]. The basis corresponds to the eigenstates of the Dicke model's integrable limit $\omega_0 \to 0$. We write it as $|N;j,m'\rangle$, where m' are the eigenvalues of J_x and N is the eigenvalue of the $A^\dagger A$ operator, with $A = a + \frac{2\gamma}{\sqrt{N}\omega}J_x$,

$$|N;j,m'\rangle = \frac{1}{\sqrt{N!}}(A^\dagger)^N|N=0;j,m'\rangle. \tag{B1}$$

The vacuum for a given m' is a boson coherent state ($|\alpha\rangle$) times an eigenstate of the J_x operator:

$$|N=0;j,m'\rangle = \left|\alpha = -\frac{2\gamma m'}{\omega\sqrt{N}}\right\rangle |jm'\rangle.$$

Now, the kth excited-state wave function of the Dicke Hamiltonian can be written as

$$|\Psi^k(N_{\max})\rangle = \sum_{N=0}^{N_{\max}}\sum_{m'=-j}^{j} C^k_{N,m'}|N;j,m'\rangle. \tag{B2}$$

Here $C^k_{N,m'}$ are the coefficients of the kth wave function in terms of the extended bosonic coherent basis and $N_{\max}$ is the value of the truncation or cutoff in the number of displaced excitations ($0 \leqslant N \leqslant N_{\max}$). The probability P_N of having N excitations in the kth state is

$$P^k_N = |\langle N|\Psi^k\rangle|^2 = \sum_{m'}\left|C^k_{N,m'}\right|^2. \tag{B3}$$

We define the departure for exact precision in the calculated wave function as [41]

$$\Delta P^k = \sum_{m'=-j}^{j}\left|C^k_{N_{\max}+1,m'}\right|^2. \tag{B4}$$

By diagonalizing the Hamiltonian with several truncations, we consider that the solution has converged if ΔP^k is smaller than certain tolerance, $N_{\max}$ being the minimum value of the truncation necessary for obtaining the numerical solution to the desired precision.

[1] R. H. Dicke, Phys. Rev. **93**, 99 (1954).
[2] D. Schneble, Y. Torii, M. Boyd, E. W. Streed, D. E. Pritchard, and W. Ketterle, Science **300**, 475 (2003).
[3] M. Scheibner, T. Schmidt, L. Worschech, A. Forchel, G. Bacher, T. Passow, and D. Hommel, Nat. Phys. **3**, 106 (2007).
[4] A. Blais, R-S. Huang, A. Wallraff, S. M. Girvin, and R. J. Schoelkopf, Phys. Rev. A **69**, 062320 (2004).
[5] J. M. Fink, R. Bianchetti, M. Baur, M. Göppl, L. Steffen, S. Filipp, P. J. Leek, A. Blais, and A. Wallraff, Phys. Rev. Lett. **103**, 083601 (2009).
[6] K. Hepp and E. H. Lieb, Ann. Phys. (NY) **76**, 360 (1973).
[7] Y. K. Wang and F. T. Hioe, Phys. Rev. A **7**, 831 (1973).
[8] E. Nahmad-Achar, O. Castaños, R. López-Peña, and J. G. Hirsch, Phys. Scr. **87**, 038114 (2013).
[9] C. Emary and T. Brandes, Phys. Rev. E **67**, 066203 (2003); Phys. Rev. Lett. **90**, 044101 (2003).
[10] N. Lambert, C. Emary, and T. Brandes, Phys. Rev. Lett. **92**, 073602 (2004).
[11] J. Vidal and S. Dusuel, Europhys. Lett. **74**, 817 (2006).
[12] K. Baumann, C. Guerlin, F. Brennecke, and T. Esslinger, Nature (London) **464**, 1301 (2010).
[13] K. Baumann, R. Mottl, F. Brennecke, and T. Esslinger, Phys. Rev. Lett. **107**, 140402 (2011).
[14] D. Nagy, G. Kónya, G. Szirmai, and P. Domokos, Phys. Rev. Lett. **104**, 130401 (2010).
[15] J. M. Knight, Y. Aharonov, and G. T. C. Hsieh, Phys. Rev. A **17**, 1454 (1978).
[16] I. Bialynicki-Birula and K. Rzaznewski, Phys. Rev. A **19**, 301 (1979).
[17] K. Gawedzki and K. Rzaznewski, Phys. Rev. A **23**, 2134 (1981).
[18] G. Liberti and R. L. Zaffino, Phys. Rev. A **70**, 033808 (2004).
[19] P. Nataf and C. Ciuti, Nat. Commun. **1**, 72 (2010).
[20] O. Viehmann, J. von Delft, and F. Marquardt, Phys. Rev. Lett. **107**, 113602 (2011).
[21] C. Ciuti and P. Nataf, Phys. Rev. Lett. **109**, 179301 (2012).
[22] Q. H. Chen, Y. Y. Zhang, T. Liu, and K. L. Wang, Phys. Rev. A **78**, 051801 (2008); T. Liu, Y. Y. Zhang, Q. H. Chen, and K. L. Wang, *ibid.* **80**, 023810 (2009).

[23] O. Castaños, E. Nahmad-Achar, R. López-Peña, and J. G. Hirsch, Phys. Rev. A **83**, 051601(R) (2011).
[24] O. Castaños, E. Nahmad-Achar, R. López-Peña, and J. G. Hirsch, Phys. Rev. A **84**, 013819 (2011).
[25] J. G. Hirsch, O. Castaños, E. Nahmad-Achar, and R. López-Peña, Phys. Scr. **87**, 038106 (2013).
[26] P. Pérez-Fernández, A. Relaño, J. M. Arias, P. Cejnar, J. Dukelsky, and J. E. García-Ramos, Phys. Rev. E **83**, 046208 (2011).
[27] M. A. Caprio, P. Cejnar, and F. Iachello, Ann. Phys. **323**, 1106 (2008).
[28] P. Cejnar, M. Macek, S. Heinze, J. Jolie, and J. Dobeš, J. Phys. A **39**, L515 (2006).
[29] A. Relaño, J. M. Arias, J. Dukelsky, J. E. García-Ramos, and P. Pérez-Fernández, Phys. Rev. A **78**, 060102 (2008); P. Pérez-Fernández, A. Relaño, J. M. Arias, J. Dukelsky, and J. E. García-Ramos, *ibid*. **80**, 032111 (2009).
[30] P. Pérez-Fernández, P. Cejnar, J. M. Arias, J. Dukelsky, J. E. García-Ramos, and A. Relaño, Phys. Rev. A **83**, 033802 (2011).
[31] T. Brandes, Phys. Rev. E **88**, 032133 (2013).
[32] M. A. Bastarrachea-Magnani and J. G. Hirsch, Rev. Mex. Fis. S **57**, 69 (2011).
[33] M. A. Bastarrachea-Magnani and J. G. Hirsch, AIP Conf. Proc. **1488**, 418 (2012).
[34] M. A. Bastarrachea-Magnani, S. Lerma-Hernández, and J. G. Hirsch, Phys. Rev. A **89**, 032102 (2014).
[35] M. Tavis and F. W. Cummings, Phys. Rev. **170**, 379 (1968).
[36] M. A. M. de Aguiar, K. Furuya, C. H. Lewenkopf, and M. C. Nemes, Ann. Phys. **216**, 291 (1992).
[37] O. Castaños, R. López-Peña, E. Nahmad-Achar, J. G. Hirsch, E. López-Moreno, and J. E. Vitela, Phys. Scr. **79**, 065405 (2009); O. Castaños, E. Nahmad-Achar, R. López-Peña, and J. G. Hirsch, *ibid*. **80**, 055401 (2009).
[38] A. Baksic and C. Ciuti, arXiv:1310.3780.
[39] Y. Yi-Xiang, J. Ye, and W.-M. Liu, Sci. Rep. **3**, 3476 (2013).
[40] M. C. Gutzwiller, *Chaos in Classical and Quantum Mechanics* (Springer, New York, 1990).
[41] J. G. Hirsch and M. A. Bastarrachea-Magnani, Phys. Scr. T (to be published), arXiv:1312.1954.